

SDSS J0806+2006 and SDSS J1353+1138: Two New Gravitationally Lensed Quasars from the Sloan Digital Sky Survey

Naohisa Inada,¹ Masamune Oguri,^{2,3} Robert H. Becker,^{4,5} Richard L. White,⁶ Michael D. Gregg,^{4,5} Paul L. Schechter,⁷ Yozo Kawano,⁸ Christopher S. Kochanek,⁹ Gordon T. Richards,¹⁰ Donald P. Schneider,¹¹ J. C. Barentine,¹² Howard J. Brewington,¹² J. Brinkmann,¹² Michael Harvanek,¹² S. J. Kleinman,¹² Jurek Krzesinski,^{12,13} Dan Long,¹² Eric H. Neilsen, Jr.,¹⁴ Atsuko Nitta,¹² Stephanie A. Snedden,¹² and Donald G. York^{15,16}

ABSTRACT

We report the discoveries of two, two-image gravitationally lensed quasars selected from the Sloan Digital Sky Survey: SDSS J0806+2006 at $z_s = 1.540$

¹Institute of Astronomy, Faculty of Science, University of Tokyo, 2-21-1 Osawa, Mitaka, Tokyo 181-0015, Japan.

²Princeton University Observatory, Peyton Hall, Princeton, NJ 08544.

³Department of Physics, University of Tokyo, Hongo 7-3-1, Bunkyo-ku, Tokyo 113-0033, Japan.

⁴IGPP-LLNL, L-413, 7000 East Avenue, Livermore, CA 94550.

⁵Physics Department, University of California, Davis, CA 95616.

⁶Space Telescope Science Institute, 3700 San Martin Drive, Baltimore, MD 21218.

⁷MIT Kavli Institute for Astrophysics and Space Research, 77 Massachusetts Avenue, Cambridge MA 02139.

⁸Department of Physics and Astrophysics, Nagoya University, Chikusa-ku, Nagoya 464-8062, Japan.

⁹Department of Astronomy, The Ohio State University, Columbus, OH 43210.

¹⁰Department of Physics and Astronomy, The Johns Hopkins University, 3400 North Charles Street, Baltimore, MD 21218-2686.

¹¹Department of Astronomy and Astrophysics, The Pennsylvania State University, 525 Davey Laboratory, University Park, PA 16802.

¹²Apache Point Observatory, P.O. Box 59, Sunspot, NM 88349.

¹³Mt. Suhora Observatory, Cracow Pedagogical University, ul. Podchorazych 2, 30-084 Cracow, Poland.

¹⁴Fermi National Accelerator Laboratory, P.O. Box 500, Batavia, IL 60510.

¹⁵Department of Astronomy and Astrophysics, The University of Chicago, 5640 South Ellis Avenue, Chicago, IL 60637.

¹⁶Enrico Fermi Institute, The University of Chicago, 5640 South Ellis Avenue, Chicago, IL 60637.

and SDSS J1353+1138 at $z_s = 1.629$ with image separations of $\Delta\theta = 1''.40$ and $\Delta\theta = 1''.41$ respectively. Spectroscopic and optical/near-infrared imaging follow-up observations show that the quasar images have identical redshifts and possess extended objects between the images that are likely to be lens galaxies at $z_l \simeq 0.6$ in SDSS J0806+2006 and $z_l \simeq 0.3$ in SDSS J1353+1138. The field of SDSS J0806+2006 contains several nearby galaxies that may significantly perturb the system, and SDSS J1353+1138 has an extra component near its Einstein ring that is probably a foreground star. Simple mass models with reasonable parameters reproduce the quasar positions and fluxes of both systems.

Subject headings: gravitational lensing — quasars: individual (SDSS J080623.70+200631.9, SDSS J135306.35+113804.8)

1. Introduction

Since the discovery of Q0957+561 (Walsh et al. 1979), about 80 gravitationally lensed quasars have been discovered (Kochanek et al. 2004). Lensed quasars are not only intriguing phenomena but also have become indispensable astronomical tools, including probes of the cosmological parameters and the structure of galaxies (e.g., Refsdal 1964; Kochanek 1991). In particular, the abundance of gravitational lenses in a well-defined source sample can be used to constrain dark energy (e.g., Turner 1990; Fukugita et al. 1990; Chae et al. 2002). Unfortunately, the largest existing survey, the Cosmic Lens All-Sky Survey (CLASS; Myers et al. 2003; Browne et al. 2003), contains only 22 lensed radio sources (with a well-defined statistical sample of 13 lenses) discovered from $\sim 10,000$ radio sources, which is still insufficient to place tight constraints on dark energy models. The Sloan Digital Sky Survey (SDSS; York et al. 2000) should lead to a significantly larger lens sample for attacking the dark energy problem. SDSS is expected to identify 10^5 quasars spectroscopically (e.g., Schneider et al. 2005) and $\approx 10^6$ quasars photometrically (e.g., Richards et al. 2004), which should lead to a sample of over 10^2 lensed quasars given a standard lensing probability of 10^{-3} (Turner et al. 1984). Indeed, 12 new lensed quasars have been discovered from the SDSS quasars so far (Inada et al. 2003a,b,c, 2005; Johnston et al. 2003; Morgan et al. 2003; Pindor et al. 2004, 2005; Oguri et al. 2004, 2005; Burles et al. 2005), in addition to recovering 5 previously known lensed quasars (Walsh et al. 1979; Weymann et al. 1980; Surdej et al. 1987; Bade et al. 2003; Oscoz et al. 1997). We can presently construct a well-defined statistical sample of 16 lensed SDSS quasars, but there remain many promising SDSS lensed quasar candidates for which the necessary follow-up observations are incomplete.

In this paper, we report on the discovery of two more gravitationally lensed quasars,

SDSS J080623.70+200631.9 (SDSS J0806+2006) and SDSS J135306.35+113804.7 (SDSS J1353+1138). We present imaging and spectroscopic follow-up observations with the University of Hawaii 2.2-meter (UH88) telescope, the W. M. Keck Observatory’s Keck I and II telescopes, and the Magellan Consortium’s Landon Clay 6.5-m (LC6.5m) telescope ¹. We model the systems to check that their geometries are consistent with the lensing hypothesis.

The structure of this paper is as follows. We describe our lens candidate selections from the SDSS data in §2. The follow-up observations and mass modeling of SDSS J0806+2006 and SDSS J1353+1138 are presented in §3 and §4, respectively. We finally present a summary and give a conclusion in §5. Throughout the paper we assume a cosmological model with the matter density $\Omega_M = 0.27$, cosmological constant $\Omega_\Lambda = 0.73$, and Hubble constant $h = H_0/100\text{km sec}^{-1}\text{Mpc}^{-1} = 0.7$ (Spergel et al. 2003).

2. Selecting Lensed Quasar Candidates from the SDSS

The SDSS is conducting a photometric and spectroscopic survey of 10,000 square degrees of the sky approximately centered on the North Galactic Cap using the dedicated wide-field (3° field of view) 2.5-m telescope (Gunn et al. 2005) at the Apache Point Observatory in New Mexico, USA. Photometric observations (Gunn et al. 1998; Lupton et al. 1999; Tucker et al. 2005) are made in five optical filters (Fukugita et al. 1996). After automated data processing by the photometric pipeline (Lupton et al. 2001; Lupton 2005), quasar and galaxy candidates are selected by the spectroscopic target selection algorithms (Eisenstein et al. 2001; Richards et al. 2002; Strauss et al. 2002). Spectra of these candidates are obtained according to the tiling algorithm of (Blanton et al. 2003) using a multi-fiber spectrograph covering 3800 Å to 9200 Å at a resolution of $R \sim 1800$. The data are very homogeneous, with an astrometric accuracy better than about $0''.1$ rms per coordinate (Pier et al. 2003) and photometric zeropoint errors less than about 0.03 magnitude over the entire survey area (Hogg et al. 2001; Smith et al. 2002; Ivezić et al. 2004). The data have been released continuously to the public (Stoughton et al. 2002; Abazajian et al. 2003, 2004, 2005; Adelman-McCarthy 2005).

We selected the two objects, SDSS J0806+2006 and SDSS J1353+1138, as lensed quasar candidates from the SDSS spectroscopic quasar sample with the same algorithm used for the

¹The second telescope of the Magellan Project; a collaboration between the Observatories of the Carnegie Institution of Washington (OCIW), University of Arizona, Harvard University, University of Michigan, and Massachusetts Institute of Technology (MIT) to construct two 6.5 Meter optical telescopes in the southern hemisphere.

discovery of most SDSS lensed quasars (e.g., Inada et al. 2003a). Specifically, the algorithm uses the SDSS image parameters `dev_L`, `exp_L` and `star_L` for the likelihood that a source can be modeled as a de Vaucouleurs profile, an exponential disk or a point source to quantify the structure of each quasar. Lensed quasars should be modeled poorly by all three profiles, so quasars with small values for all three likelihoods are good lens candidates (see Inada et al. 2003a, for more details).

The SDSS *i*-band images of SDSS J0806+2006 and SDSS J1353+1138 are shown in Figure 1. Both systems are clearly resolved, making them excellent lens candidates since their spectra are clearly those of $z > 1$ quasars. For SDSS J0806+2006, the total magnitudes (within $\sim 2''.3$ aperture radius) of the system are 19.18 ± 0.05 , 18.76 ± 0.01 , 18.44 ± 0.02 , 18.06 ± 0.02 , and 17.92 ± 0.05 , in *u*, *g*, *r*, *i*, and *z*, respectively. For SDSS J1353+1138, the total magnitudes (*ugriz*, within $\sim 2''.1$ aperture radius) are 16.87 ± 0.01 , 16.60 ± 0.01 , 16.48 ± 0.01 , 16.26 ± 0.01 , and 16.20 ± 0.02 , respectively. The redshifts of SDSS J0806+2006 and SDSS J1353+1138 measured from their SDSS spectra are $z_s = 1.537 \pm 0.002$ and $z_s = 1.623 \pm 0.003$, respectively. From the SDSS spectra, with a fiber aperture of $3''.0$, we know that the components of the candidates cannot have greatly dissimilar spectra. However, we cannot resolve the spectra of the individual components.

Thus, while the SDSS data are sufficient to identify these objects as lens candidates, additional observations are needed to confirm them as lensed quasars. Deeper and higher resolution images are needed to confirm the existence of multiple quasar images and to search for the lens galaxies, and spatially resolved spectra are needed to confirm that the quasar images have identical redshifts. We present this evidence for SDSS J0806+2006 in §3 and for SDSS J1353+1138 in §4.

3. SDSS J0806+2006

3.1. Imaging Observations

We obtained *V*, *R* and *I*-band images of SDSS J0806+2006 using the 8k mosaic CCD camera at the UH88 telescope, on 2004 December 16. The pixel scale of the 8k mosaic CCD camera is $0''.235 \text{ pixel}^{-1}$. The exposure time was 360 sec for each band. The typical seeing in the exposures was $\sim 0''.7$, about a half of the typical seeing size of the SDSS ($\sim 1''.5$). Bias-subtracted and flat-field corrected images are shown in the upper panels of Figure 2. We also obtained an *H*-band image using the QUick InfraRed Camera (QUIRC) of the UH88 telescope on 2005 February 21 and a *K'*-band image using the Near InfraRed Camera (NIRC; Matthews & Soifer 1994) of the Keck I telescope on 2005 April 24. The pixel scale of QUIRC

is $0''.189 \text{ pixel}^{-1}$, and that of the NIRC is $0''.15 \text{ pixel}^{-1}$. The seeing was $\sim 0''.7$ in the QUIRC observation, and it was $\sim 0''.4$ in the NIRC observation. The total exposure time was 720 sec and 900 sec for H -band imaging and K' -band imaging, respectively. The H -band image is shown in Figure 2, and the K' -band image is shown in Figure 3.

All the images ($VRIHK'$) clearly show two stellar components; we name these two stellar components A (eastern component) and B (western component), with A being the brighter component. To determine if there are any extended objects in between the stellar components, we subtracted point spread functions (PSFs) from the raw $VRIH$ images, adopting a nearby star as a template for the PSF. The results are shown in the lower panels of Figure 2; there is clearly residual flux between components A and B in all four images. This object (named G) is quite red, with colors of $V - R \sim 1.1$ and $R - I \sim 1.1$ that are similar to those of an early-type galaxy at $z_l \sim 0.6$ (Fukugita et al. 1995). Such a redshift is consistent with the redshift of a Mg II absorption line system in the spectra of the quasars (see §3.2) and an estimate based on the Faber-Jackson relation (see §3.3). Therefore, we conclude that component G is the lens galaxy. In the higher resolution NIRC K' -band image (left panel of Figure 3), we can identify component G between components A and B even before PSF subtraction. We fit this image using GALFIT (Peng et al. 2002) to find that G is well-modeled by a de Vaucouleurs profile of ellipticity $e = 0.18$ and major axis position angle $\theta_e = 51^\circ$.

The astrometry and photometry of components A, B and G are summarized in Table 1. The optical images were calibrated using the standard star PG 0231+051 (Landolt 1992) and the H -band image was calibrated using the standard star FS 21 (Hawarden et al. 2001). We lack a photometric standard stars for the NIRC K' -band image, thus the data were used only for astrometry and the flux ratio constraints in the lens models. When we fit the NIRC K' -band image using a model consisting of the two quasar images and the lens galaxy, we find a quasar flux ratio of 0.53 as compared to the mean flux ratio of 0.67 (derived from fitting only the PSF models) for the optical bands that could be created by a modest amount of dust extinction or chromatic microlensing. We report the astrometry from using GALFIT to simultaneously fit components A, B and G in the NIRC K' -band image. The angular separation of components A and B is $1''.403 \pm 0''.012$.

3.2. Spectroscopic Observations

A spectroscopic observation of SDSS J0806+2006 was conducted with the Keck II telescope on 2005 April 12 in $\sim 1''.0$ seeing. We used the echellette mode of the Echellette Spectrograph and Imager (ESI; Sutin 1997; Sheinis et al. 2002) with the MIT-LL

2048×4096 CCD camera. The spectral range was 3900 Å to 11,000 Å at a spectral resolution of 11.4 km s⁻¹pixel⁻¹ (R~27000). The exposure time was 900 sec. The 1''0-wide slit was oriented to observe components A and B simultaneously. The spectra of each component was extracted using the standard method (summing the fluxes in a window around the position of each component and subtracting the sky using neighboring windows on either side of the trace). We show the binned spectra in Figure 4. Both spectra have the C III] and Mg II emission lines at the same wavelength, with an estimated velocity difference of 20±70 km s⁻¹ for the Mg II emission line. We summarize the redshifts calculated from these emission lines in Table 2. In addition, the spectral energy distributions (SEDs) are also very similar. The ratio of the spectra, which is shown in Figure 4, is almost constant (~0.7) for a wide range of wavelengths, and it is consistent with the mean flux ratio of the optical images (0.67). Note, however, that the emission line flux ratios appear to differ slightly from that of the continuum, suggesting that there is some microlensing of the continuum by the stars in the lens galaxy.

In addition to the quasar emission lines, we found a strong Mg II absorption line system at $z = 0.573$ in both spectra (see the inset of Figure 4). We also found Ca II H and K (~ 6200 Å) and Fe II absorption lines (~ 4100 Å) at $z = 0.573$ in the spectra. The fact that the redshift of this absorption line system is close to the estimated redshift (see §3.1) of the probable lens galaxy (component G) and that Mg II absorption lines are frequently associated with galaxies (e.g., Bergeron & Boisse 1991) suggests that the absorption is due to the lens galaxy. If this is the case, the lens redshift should be $z_l \simeq 0.573$; we adopt this value for the mass models presented in the next subsection.

3.3. Mass Modeling

To explore the lensing hypothesis further, we modeled the system using the two standard mass models: a Singular Isothermal Sphere with an external shear (SIS+shear) model, and a Singular Isothermal Ellipsoid (SIE) model. Both models have eight parameters: the Einstein radius R_E , the shear γ or ellipticity e and its position angle (θ_γ or θ_e), the position of the lens galaxy, and the position and flux of the source quasar. We have only eight constraints (the positions of A, B and G, and the fluxes of A and B), so we should be able to fit the data perfectly. We should, however, be able to do so with sensible values for the shear or ellipticity of the models. We used the component positions from Table 1 and the flux ratio of 0.53 derived from the GALFIT model of the NIRC K' -band image including the two stellar components and the lens galaxy.

We used *lensmodel* (Keeton 2001b) to determine the model parameters, with the results

summarized in Table 3. The required ellipticities of $\gamma = 0.03$ or $e = 0.08$ are typical of other lensed systems and roughly consistent with that of the lens galaxy ($e = 0.18$), but there is a significant misalignment between the position angle of the major axis of the models ($\theta_e \simeq -28^\circ$) and that of the lens galaxy ($\theta_e = 51^\circ$). This might imply that the system is affected by a strong external perturbation (Keeton et al. 1998). Indeed, there are at least four galaxies within a $16''$ radius of the lens (named G1–4, with the nearest galaxy only $4''$ from the lens; see Table 4), so the position angle of the models may be a compromise between that of the lens galaxy and the shear induced by G1. Finally, these models predict that the time delay between the images is $\sim 32h^{-1}$ days.

We can estimate the redshift of the lens galaxy based on the Faber-Jackson relation (Faber & Jackson 1976). From the Table 3 of Rusin et al. (2003), we estimate that the lens magnitude should be $R \sim 20.5$ for $\Delta\theta = 1''.40$, $z_s = 1.54$, and assuming $z_l = 0.57$. While this is somewhat brighter than the observed R -band magnitude of galaxy G ($R = 21.2$), it is roughly consistent given the ± 0.6 mag scatter (Rusin et al. 2003). The rough agreement of this estimate further supports for a lens galaxy redshift of $z_l \simeq 0.573$.

4. SDSS J1353+1138

4.1. Imaging Observations

We obtained V , R , and I -band images of SDSS J1353+1138 using the 8K mosaic CCD camera of the UH88 telescope on 2004 May 25 in $\sim 1''.0$ seeing. The exposure times were 120 sec for V and 180 sec for R and I , respectively. We also acquired an H -band image on the UH88 telescope using QUIRC on 2005 February 21. The exposure time was 720 sec, and the seeing was $\sim 0''.7$. The images, shown in the upper panels of Figure 5, clearly show two stellar components, which we named A (northern and brighter component) and B (southern component). Although it is not obvious in the raw H -band image of Figure 5, an extended object can be seen between components A and B even before the PSF subtraction. We also obtained g and i -band images using the Magellan Instant Camera (MagIC) at the LC6.5m telescope on 2005 April 15. The pixel scale of MagIC is $0''.069 \text{ pixel}^{-1}$. The seeing was $\sim 0''.6$, and the exposure time was 360 sec for g -band and 480 sec for i -band.

After subtracting PSF models for the two stellar components, we clearly detect an extended red object positioned between them in all the residual images. These residual images are shown in Figure 5 and 6 for the UH88 and Magellan data, respectively. We identify this extended object, which we denote as G, with the lens galaxy. We fit the i -band image using GALFIT to find that the lens galaxy is well-modeled with a de Vaucouleurs

profile of ellipticity $e = 0.50$ and major axis position angle $\theta_e = -62^\circ$. In addition to component G, there is an additional object which we named component C near image A. It is most easily seen in the g -band image after subtracting components A and B (see the middle panel of Figure 6), but it can also be seen at the same position in the i -band image.

There are four possible interpretations of component C. First, it could be a chance superposition of a foreground star. It is well fit by the PSF (see the bottom panels of Figure 6), and our lens models require only components A, B and G to reproduce the system with reasonable parameter values (see 4.3). Second, it could be an object related to the lens galaxy. However, lens models with significant extra mass at the position of component C generally fit the data very badly. Third, it could be a third image of the quasar. This seems unlikely since its colors are very different from components A and B (see Table 5). Moreover, identifying it as a quasar image makes little sense as a lens geometry since it is in the wrong place to be a central, odd image (which should lie between components B and G) or to be part of a four-image system in which one of the A/B/C components is an unresolved image pair. Fourth, it could be emission from the host galaxy of the source quasar. Probably only the first possibility is permitted, although we cannot completely exclude the other possibilities.

We summarize astrometry and photometry of components A, B, C and G in Table 5. The optical images were calibrated using the standard stars PG 1528+062 (Landolt 1992) and SA 107-351 (Smith et al. 2002), and the H -band image was calibrated using the standard star FS 21 (Hawarden et al. 2001). The flux ratio of components A and B changes significantly with wavelength, from a mean flux ratio in the optical of 0.35 to an H -band flux ratio of 0.54. The angular separation of components A and B is $1''.406 \pm 0''.007$.

4.2. Spectroscopic Observations

We used ESI on the Keck II telescope to obtain spectra of the two components of SDSS J1353+1138 on 2005 April 12. The instrumental set up was the same as in §3.2 and we used an exposure time of 600 sec. The binned spectra are shown in Figure 7. Both components have C III] and Mg II emission lines at identical wavelengths, with a velocity difference of only 10 ± 50 km s $^{-1}$ for the Mg II emission line. We summarize the redshifts derived from the emission lines in Table 6.

The flux ratio of the spectra is nearly constant (~ 0.4) and consistent with that in the optical images (~ 0.35). There is, however, a slight increase in the ratio redwards of about 5300 Å that may be due to contamination of the spectrum of component B by emission from the lens galaxy. Assuming this feature is due to the 4000Å break of the lens galaxy, it implies

a lens redshift of $z_l \sim 0.3$. Since the colors of the lens galaxy of $V - R \sim 0.3$, $R - I \sim 1.0$, and $g - i \sim 1.1$ are roughly consistent with those of an early-type galaxy at $z = 0.1 \sim 0.3$ (Fukugita et al. 1995), we adopt $z_l = 0.3$ for mass modeling.

The quasar spectra also contain strong Mg II absorption line systems at $z = 1.238$, 0.904, and 0.637, with their Fe II absorption lines. These are unlikely to be associated with the lens galaxy, given the large difference from the lens redshift estimated from the colors, and also given the fact that many (unlensed) quasars show Mg II absorption. We note that an Mg II absorption line due to a $z \simeq 0.3$ lens is undetectable in our spectra because it would lie beyond the atmospheric cutoff.

4.3. Mass Modeling

We modeled SDSS J1353+1138 in the same way as in §3.3. The positions of the quasars and lens galaxy are taken from Table 7 (neglecting component C). For the flux ratio of components A and B, we adopt 0.31, which was derived from the GALFIT model of the MagIC i -band image. The results are summarized in Table 7. The derived shear and ellipticity of $\gamma = 0.05$ and $e = 0.15$, are again typical for a lensed quasar system. The derived ellipticity (0.15) appears to be significantly smaller than the ellipticity of the observed light profile ($e=0.50$), but this difference is commonly seen in the lensed quasar systems (Keeton et al. 1998). However, in addition to the disagreement of the ellipticity, there is a significant misalignment between the position angle of the models ($\theta_e \simeq -34^\circ$) and that of the lens galaxy ($\theta_e = -62^\circ$). While this might be due to external perturbations, there are no nearby galaxies that can easily explain the misalignment. It could be due to component C, but we find that simple tests of lens models with mass located at the position of component C generally fail to fit the data. The time delay between A and B is predicted to be $\sim 16h^{-1}$ days, assuming the lens redshift of $z_l = 0.3$.

As in §3.3 we also estimated the lens redshift based on the Faber-Jackson relation. Again we used Table 3 of Rusin et al. (2003), $\Delta\theta = 1''.41$, and $z_s=1.63$ to estimate that the lens magnitude should be $R \sim 19.2$, assuming $z_l = 0.3$. This estimate is in rough agreement with the observed R -band magnitude of galaxy G ($R = 18.8$), again supporting for a lens redshift of $z_l \sim 0.3$.

5. Summary

We report the discovery of two doubly-imaged quasar lenses, SDSS J0806+2006 and SDSS 1353+1138. Both were selected from the SDSS spectroscopic quasar sample as lensed quasar candidates and confirmed in subsequent imaging and spectroscopic observations. SDSS J0806+2006 consists of two $z_s = 1.540$ quasar images separated by $\Delta\theta = 1''.40$ lensed by a galaxy at $z_l \simeq 0.6$. The lens galaxy is closer to the fainter image as expected, and its redshift, as suggested by its magnitude, colors, and the presence of a Mg II absorption feature, is $z_l = 0.573$. Several nearby galaxies may perturb this system and indicate that the lens galaxy is part of a small group. SDSS 1353+1138 consists of two $z_s = 1.629$ quasar images separated by $\Delta\theta = 1''.41$ with a lens galaxy at $z_l \sim 0.3$. The redshift of the lens galaxy is estimated based on its magnitude, colors, and the spectral flux ratio between the two quasar images. There is an additional component, which we have labeled C, superposed on this system whose nature is presently unexplained. Observations using the *Hubble Space Telescope* are probably required to clarify its role in the lensed quasar system.

N. I. and M. O. are supported by JSPS through JSPS Research Fellowship for Young Scientists. A portion of this work was also performed under the auspices of the U.S. Department of Energy, National Nuclear Security Administration by the University of California, Lawrence Livermore National Laboratory under contract No. W-7405-Eng-48.

Some of the data presented herein were obtained at the W.M. Keck Observatory, which is operated as a scientific partnership among the California Institute of Technology, the University of California and the National Aeronautics and Space Administration. The Observatory was made possible by the generous financial support of the W.M. Keck Foundation.

Funding for the creation and distribution of the SDSS Archive has been provided by the Alfred P. Sloan Foundation, the Participating Institutions, the National Aeronautics and Space Administration, the National Science Foundation, the U.S. Department of Energy, the Japanese Monbukagakusho, and the Max Planck Society. The SDSS Web site is <http://www.sdss.org/>.

The SDSS is managed by the Astrophysical Research Consortium (ARC) for the Participating Institutions. The Participating Institutions are The University of Chicago, Fermilab, the Institute for Advanced Study, the Japan Participation Group, The Johns Hopkins University, the Korean Scientist Group, Los Alamos National Laboratory, the Max-Planck-Institute for Astronomy (MPIA), the Max-Planck-Institute for Astrophysics (MPA), New Mexico State University, University of Pittsburgh, University of Portsmouth, Princeton University, the United States Naval Observatory, and the University of Washington.

REFERENCES

- Abazajian, K., et al. 2003, *AJ*, 126, 2081
- Abazajian, K., et al. 2004, *AJ*, 128, 502
- Abazajian, K., et al. 2005, *AJ*, 129, 1755
- Adelman-McCarthy, J. K., et al. 2005, *ApJS*, in press (astro-ph/0507711)
- Bade, N., Siebert, J., Lopez, S., Voges, W., & Reimers, D. 1997, *A&A*, 317, L13
- Bergeron, J., & Boisse, P. 1991, *A&A*, 243, 344
- Blanton, M. R., Lin, H., Lupton, R. H., Maley, F. M., Young, N., Zehavi, I., & Loveday, J. 2003, *AJ*, 125, 2276
- Browne, I. W. A., et al. 2003, *MNRAS*, 341, 13
- Burles, S., et al. 2005, *AJ*, in preparation
- Chae, K.-H., et al. 2002, *Phys. Rev. Lett.*, 89, 151301
- Eisenstein, D. J., et al. 2001, *AJ*, 122, 2267
- Faber, S. M. & Jackson, R. E. 1976, *ApJ*, 204, 668
- Fukugita, M., Futamase, T., & Kasai, M. 1990, *MNRAS*, 246, 24P
- Fukugita, M., Shimasaku, K., & Ichikawa, T. 1995, *PASP*, 107, 945
- Fukugita, M., Ichikawa, T., Gunn, J. E., Doi, M., Shimasaku, K., & Schneider, D. P. 1996, *AJ*, 111, 1748
- Gunn, J. E., et al. 1998, *AJ*, 116, 3040
- Gunn, J. E., et al. 2005, *AJ*, submitted
- Hawarden, T. G., Leggett, S. K., Letawsky, M. B., Ballantyne, D. R., & Casali, M. M. 2001, *MNRAS*, 325, 563
- Hogg, D. W., Finkbeiner, D. P., Schlegel, D. J., & Gunn, J. E. 2001, *AJ*, 122, 2129
- Inada, N., et al. 2003a, *AJ*, 126, 666
- Inada, N., et al. 2003b, *AJ*, submitted

- Inada, N., et al. 2003c, *Nature*, 426, 810
- Inada, N., et al. 2005, *AJ*, 130, 1967
- Ivezić, Ž., et al. 2004, *AN*, 325, 583
- Johnston, D. E., et al. 2003, *AJ*, 126, 2281
- Keeton, C. R. 2001b, preprint (astro-ph/0102340)
- Keeton, C. R., Kochanek, C. S., & Falco, E. E. 1998, *ApJ*, 509, 561
- Kochanek, C. S. 1991, *ApJ*, 373, 354
- Kochanek, C. S., Schneider, P., Wambsganss, J., 2004, Part 2 of Gravitational Lensing: Strong, Weak & Micro, Proceedings of the 33rd Saas-Fee Advanced Course, G. Meylan, P. Jetzer & P. North, eds. (Springer-Verlag: Berlin)
- Landolt, A. U. 1992, *AJ*, 104, 340
- Lupton, R. H., Gunn, J. E., & Szalay, A. S. 1999, *AJ*, 118, 1406
- Lupton, R., Gunn, J. E., Ivezić, Z., Knapp, G. R., Kent, S., & Yasuda, N. 2001, in ASP Conf. Ser. 238, *Astronomical Data Analysis Software and Systems X*, ed. F. R. Harnden, Jr., F. A. Primini, and H. E. Payne (San Francisco: Astr. Soc. Pac.), p. 269 (astro-ph/0101420)
- Lupton, R. 2005, *AJ*, submitted
- Matthews, K., & Soifer, B. T. 1994, *ASSL Vol. 190: Astronomy with Arrays, The Next Generation*, 239
- Morgan, N. D., Snyder, J. A., & Reens, L. H. 2003, *AJ*, 126, 2145
- Myers, S. T., et al. 2003, *MNRAS*, 341, 1
- Oguri, M., et al. 2004, *PASJ*, 56, 399
- Oguri, M., et al. 2005, *ApJ*, 622, 106
- Osoz, A., Serra-Ricart, M., Mediavilla, E., Buitrago, J., & Goicoechea, L. J. 1997, *AJ*, 491, L7
- Peng, C. Y., Ho, L. C., Impey, C. D., & Rix, H.-W. 2002, *AJ*, 124, 266

- Pier, J. R., Munn, J. A., Hindsley, R. B., Hennessy, G. S., Kent, S. M., Lupton, R. H., & Ivezić, Ž. 2003, *AJ*, 125, 1559
- Pindor, B., et al. 2004, *AJ*, 127, 1318
- Pindor, B., et al. 2005, *AJ*, in press (astro-ph/0509296)
- Refsdal, S. 1964, *MNRAS*, 128, 307
- Richards, G. T., et al. 2002, *AJ*, 123, 2945
- Richards, G. T., et al. 2004, *ApJS*, 155, 257
- Rusin, D, et al. 2003, *ApJ*, 587, 143
- Schneider, D. P., et al. 2005, *AJ*, 130, 367
- Sheinis, A. I., Bolte, M., Epps, H. W., Kibrick, R. I., Miller, J. S., Radovan, M. V., Bigelow, B. C., & Sutin, B. M. 2002, *PASP*, 114, 851
- Smith, J. A., et al. 2002, *AJ*, 123, 2121
- Spergel, D. N., et al. 2003, *ApJS*, 148, 175
- Stoughton, C., et al. 2002, *AJ*, 123, 485
- Strauss, M. A., et al. 2002, *AJ*, 124, 1810
- Surdej, J., Swings, J.-P., Magain, P., Courvoisier, T. J.-L., & Borgeest, U. 1987, *Nature*, 329, 695
- Sutin, B. M. 1997, *Proc. SIPE*, 2871, 1116
- Tucker, D. L., et al. 2005, *AJ*, submitted
- Turner, E. L., Ostriker, J. P., & Gott, J. R., III 1984, *ApJ*, 284, 1
- Turner, E. L. 1990, *ApJ*, 365, L43
- Walsh, D., Carswell, R. F., & Weymann, R. J. 1979, *Nature*, 279, 381
- Weymann, R. J., et al. 1980, *Nature*, 285, 641
- York, D. G., et al. 2000, *AJ*, 120, 1579

Table 1. ASTROMETRY AND PHOTOMETRY OF SDSS J0806+2006

Object	$\Delta\text{R.A.}(\prime\prime)^{\text{a}}$	$\Delta\text{Dec.}(\prime\prime)^{\text{a}}$	V^{b}	R^{b}	I^{b}	H^{b}
A	0.000 ± 0.005	0.000 ± 0.005	19.23 ± 0.01	18.93 ± 0.01	18.54 ± 0.01	16.87 ± 0.01
B	-1.136 ± 0.007	-0.823 ± 0.007	19.82 ± 0.02	19.36 ± 0.02	18.84 ± 0.01	17.34 ± 0.02
G	-0.811 ± 0.015	-0.574 ± 0.015	22.27 ± 0.07	21.20 ± 0.04	20.16 ± 0.03	17.90 ± 0.05

^aMeasured in the Keck NIRC K' -band image using GALFIT. The celestial coordinates of component A are R.A.= $121^{\circ}59875$ and Decl.= $20^{\circ}10886$ (J2000).

^bPSF magnitudes for the stellar objects and a $2\prime\prime$ radius aperture magnitude for the extended object. The errors do not include the photometric uncertainty of the standard star or the uncertainty due to the PSF subtraction.

Table 2. EMISSION LINES OF SDSS J0806+2006 SPECTRA

Line(Å)	Component A			Component B		
	λ_{obs} (Å)	FWHM(Å)	Redshift	λ_{obs} (Å)	FWHM(Å)	Redshift
C III](1908.73)	4847.18	42.4	1.5395 ± 0.0005	4847.99	43.8	1.5399 ± 0.0007
Mg II(2798.75)	7110.25	48.2	1.5405 ± 0.0004	7109.44	52.0	1.5402 ± 0.0006

Table 3. LENS MODELING: SDSS J0806+2006

Model	$R_E(\prime)$	γ or e	θ_γ or θ_e^a	$\Delta t[h^{-1}\text{day}]^b$	μ_{tot}^c
SIS+shear	0.68	0.03	–28.0	31.6	4.63
SIE	0.69	0.08	–27.9	32.5	4.62

^aEach position angle is measured East of North.

^bThe lens redshift is assumed to be $z = 0.57$.

^cPredicted total magnification.

Table 4. POSITIONS OF GALAXIES AROUND SDSS J0806+2006

Object	$\Delta\text{R.A.}(\prime\prime)^{\text{a}}$	$\Delta\text{Dec.}(\prime\prime)^{\text{a}}$	$*/\text{G}^{\text{b}}$
G1	−3.766	0.965	0.11
G2	5.957	2.451	0.03
G3	3.480	−8.784	0.09
G4	−13.770	−7.970	0.07

^aPositions relative to component A, measured in the Keck NIRC K' -band image

^b K' -band flux ratio between each object and component G

Table 5. ASTROMETRY AND PHOTOMETRY OF SDSS J1353+1138

Object	$\Delta\text{R.A.}(\prime\prime)^{\text{a}}$	$\Delta\text{Dec.}(\prime\prime)^{\text{a}}$	V^{b}	R^{b}	I^{b}	H^{b}	g^{b}	i^{b}
A	0.000 ± 0.003	0.000 ± 0.004	17.08 ± 0.01	16.74 ± 0.01	16.44 ± 0.01	15.16 ± 0.01	16.91 ± 0.01	16.77 ± 0.01
B	-0.267 ± 0.003	-1.380 ± 0.004	18.63 ± 0.02	17.63 ± 0.01	17.43 ± 0.01	15.83 ± 0.02	18.50 ± 0.01	17.88 ± 0.01
C	0.107 ± 0.044	-0.358 ± 0.044	20.96 ± 0.06	21.67 ± 0.10
G	-0.255 ± 0.008	-1.041 ± 0.008	19.06 ± 0.03	18.80 ± 0.02	17.80 ± 0.01	16.16 ± 0.02	19.84 ± 0.01	18.77 ± 0.01

^aMeasured in the MagIC i -band image using GALFIT (except component C). The celestial coordinates of component A are R.A.= $208^{\circ}27646$ and Decl.= $11^{\circ}63467$ (J2000).

^bPSF magnitudes for the stellar objects and a $2\prime.0$ radius aperture magnitude for the extended object. The errors do not include the photometric uncertainty of the standard star or the uncertainty of the PSF subtraction.

Table 6. EMISSION LINES OF SDSS J1353+1138 SPECTRA

Line(Å)	Component A			Component B		
	λ_{obs} (Å)	FWHM(Å)	Redshift	λ_{obs} (Å)	FWHM(Å)	Redshift
C III](1908.73)	5007.61	75.6	1.6235 ± 0.0006	5008.08	75.6	1.6238 ± 0.0006
Mg II(2798.75)	7359.33	74.3	1.6295 ± 0.0004	7358.66	73.4	1.6293 ± 0.0004

Table 7. LENS MODELING: SDSS J1353+1138

Model	$R_E(\prime\prime)$	γ or e	θ_γ or θ_e^a	$\Delta t[h^{-1}\text{day}]^b$	μ_{tot}^c
SIS+shear	0.71	0.05	–35.1	16.2	3.81
SIE	0.70	0.15	–34.3	16.4	3.75

^aEach position angle is measured East of North.

^bThe lens redshift is assumed to be $z = 0.3$.

^cPredicted total magnification.

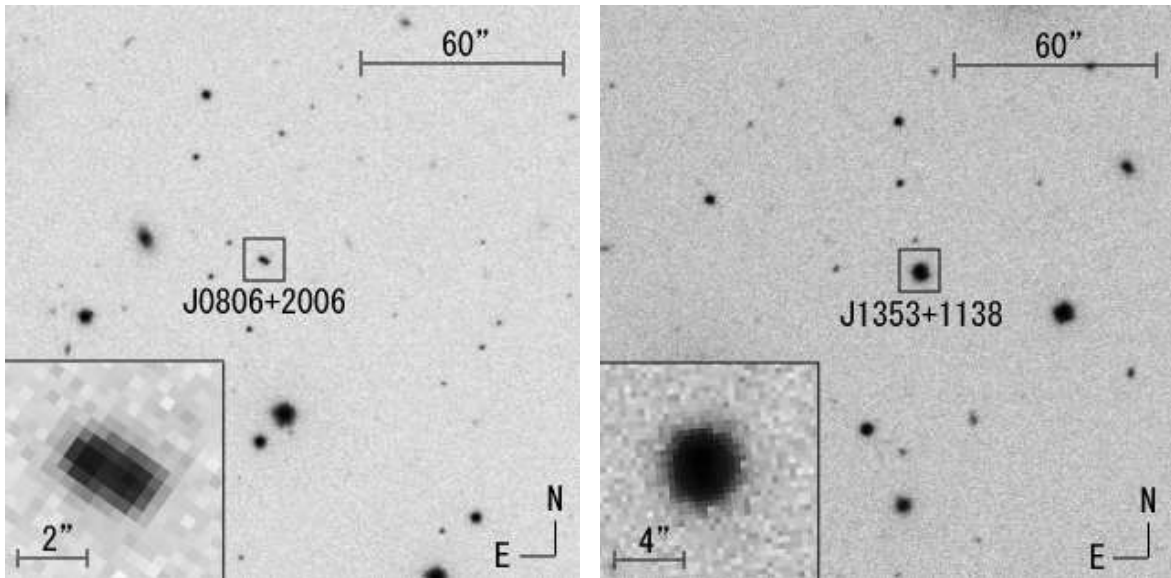


Fig. 1.— *Left*: The SDSS *i*-band image of the field centered on SDSS J0806+2006. The image scale is $0''.396 \text{ pixel}^{-1}$. The enlarged SDSS J0806+2006 image is shown in the inset. In both the field image and the inset, North is up and East is left. *Right*: Same as the left panel, but for SDSS J1353+1138.

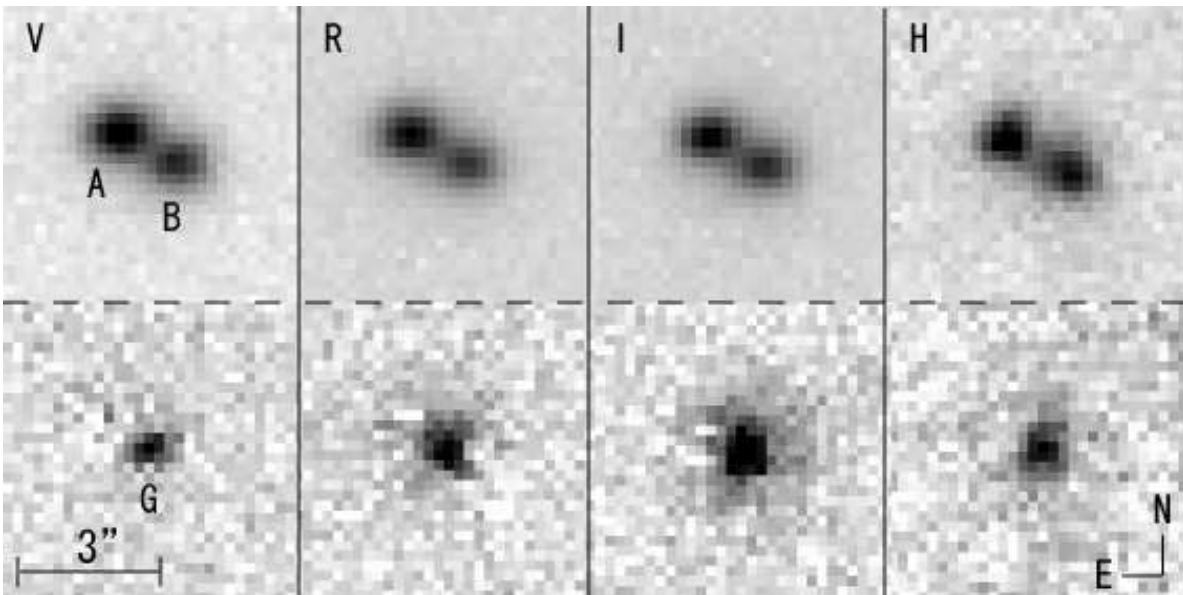


Fig. 2.— The $VRIH$ -band images of SDSS J0806+2006 taken with the 8k mosaic CCD camera and QUIRC at the UH88. The image scales are $0''.235 \text{ pixel}^{-1}$ for the 8k mosaic CCD camera and $0''.189 \text{ pixel}^{-1}$ for QUIRC. The lower panels show the images after subtracting components A and B: The images clearly show the lens galaxy (component G).

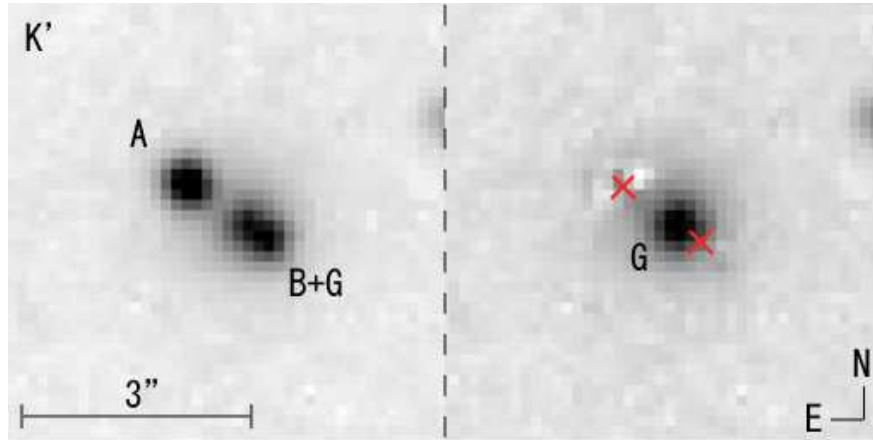


Fig. 3.— The NIRC K' -band image of SDSS J0806+2006. The image scale is $0''.15 \text{ pixel}^{-1}$. In the right panel, components A and B are subtracted. The lens galaxy can be clearly seen even before the PSF subtraction, as well as in the PSF-subtracted image.

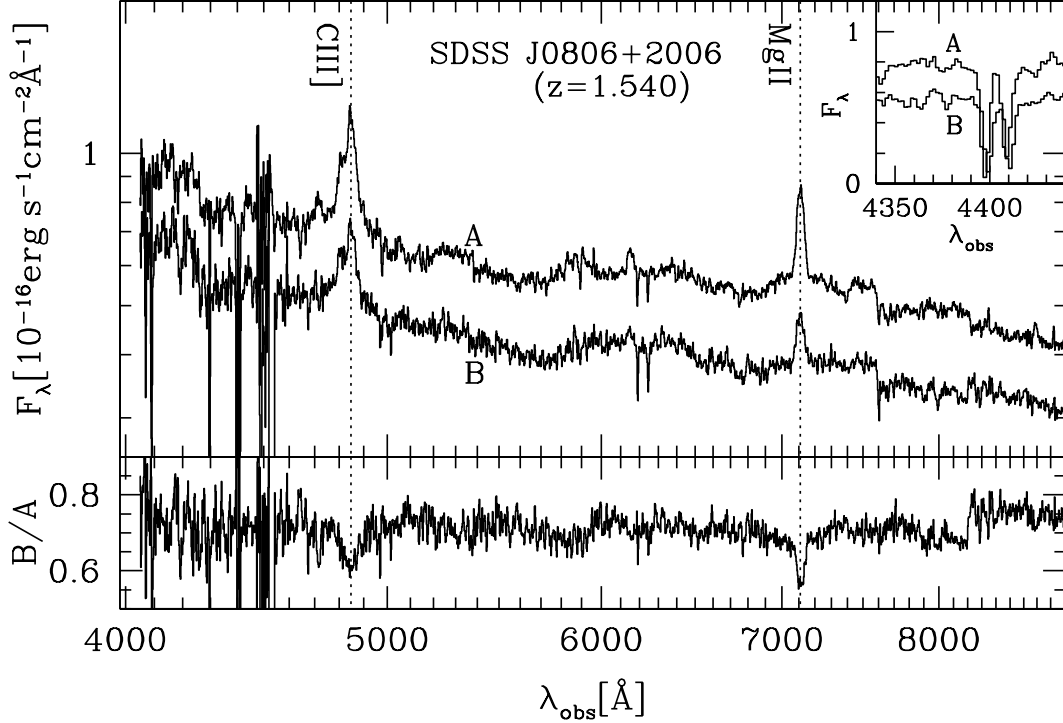


Fig. 4.— The (binned) spectra of components A and B of SDSS J0806+2006 taken with the ESI on the Keck II. The spectral resolution is $R \sim 27000$. The vertical dotted lines represent the positions of emission lines redshifted to $z = 1.534$ of C III] (1908.73 \AA) and Mg II (2798.75 \AA), respectively. Both components clearly have the identical redshift. The lower panel shows the spectral flux ratio; it is almost constant and is consistent with the mean photometric flux ratio (0.67). In the inset, we show the Mg II absorption line system at $z = 0.573$, which is probably associated with the lens galaxy. The data have bad columns around $\sim 4500 \text{ \AA}$.

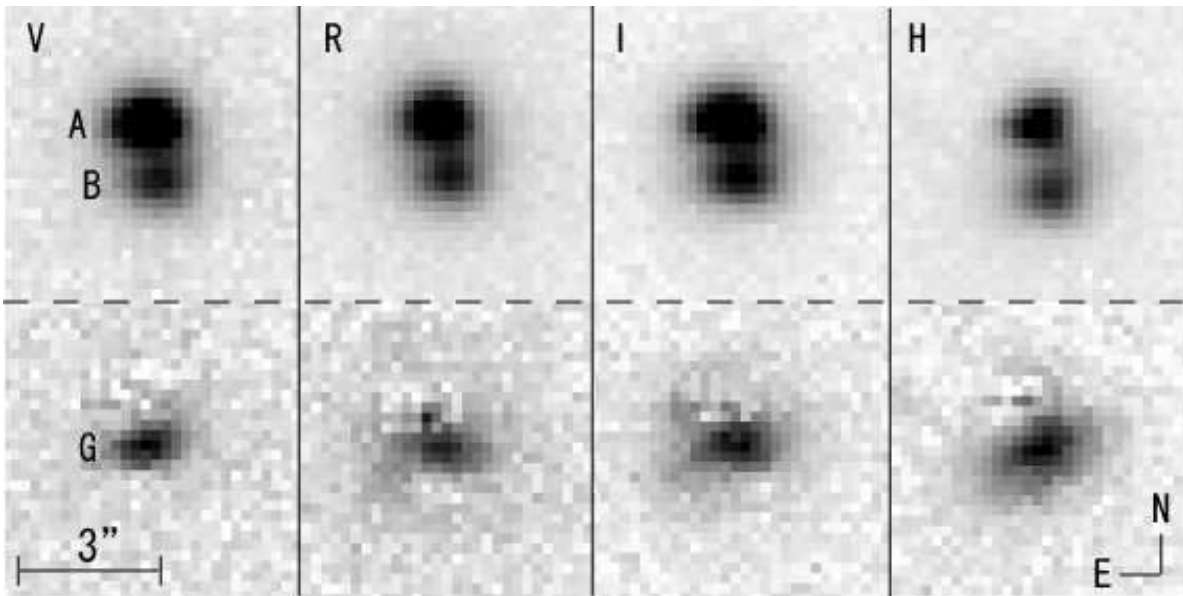


Fig. 5.— Same as Figure 2, but for SDSS J1353+1138. The lens galaxy is also clearly seen in the PSF-subtracted images.

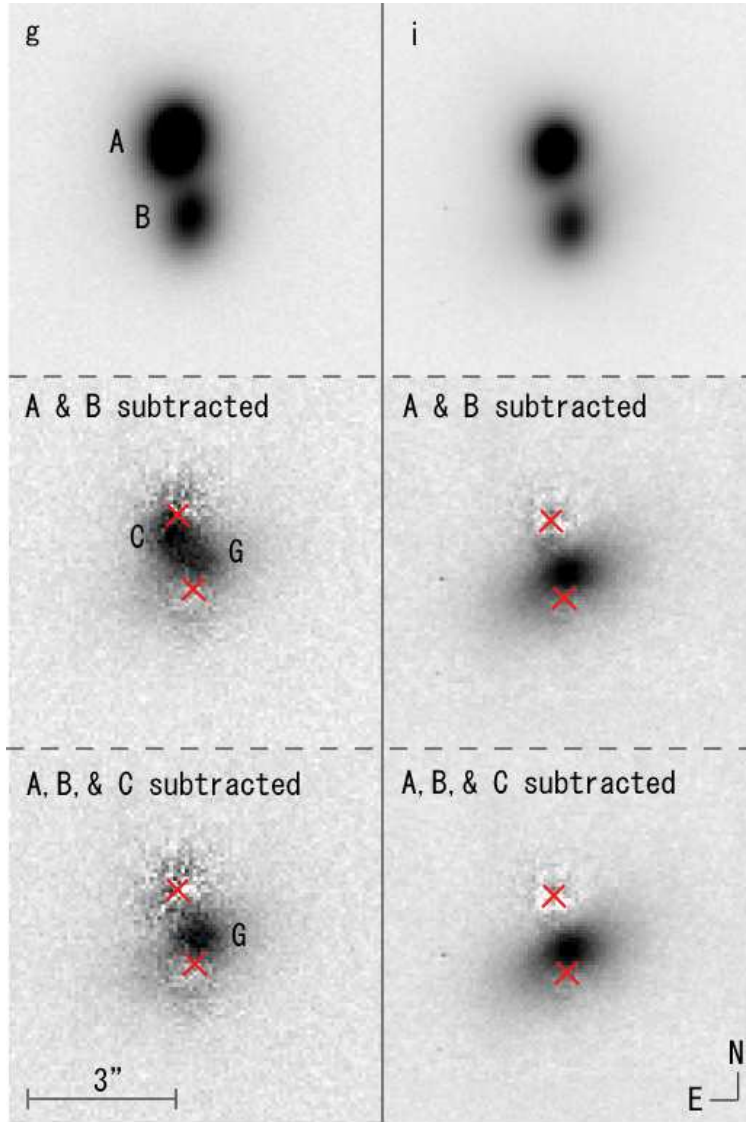


Fig. 6.— The MagIC *gi*-band images of SDSS J1353+1138. The image scale is $0''.069$ pixel $^{-1}$. The top panels show the original images, the middle panels show the residuals after subtracting components A and B, and the bottom panels show the residuals after subtracting components A, B and C. Note the relatively blue color of component C compared to the quasar images and the lens galaxy.

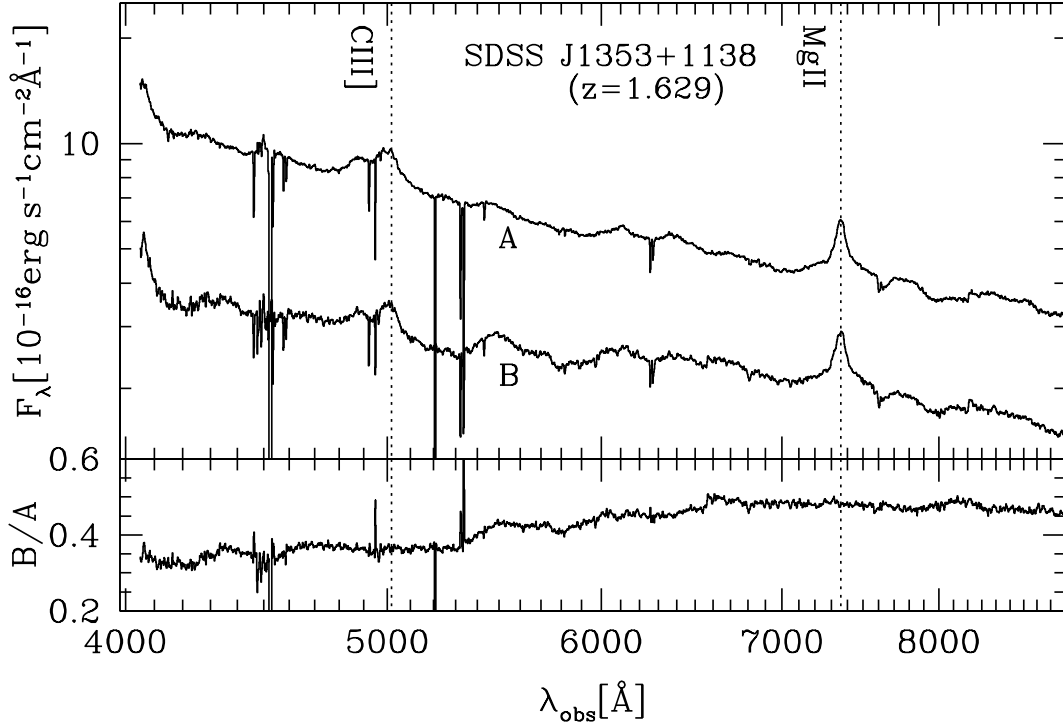


Fig. 7.— Same as Figure 4, but for the (binned) spectra of SDSS J1353+1138 are shown. The spectral resolution is $R \sim 27000$. We find that both components have the identical redshift. The spectral flux ratio is also almost constant and is consistent with the mean photometric flux ratio (0.35). There are three Mg II absorption line systems at $z = 1.238$ ($\sim 6260 \text{ \AA}$), $z = 0.904$ ($\sim 5330 \text{ \AA}$), and $z = 0.637$ ($\sim 4580 \text{ \AA}$) with their Fe II absorption lines, but they probably arise from the intervening galaxies, not the lens galaxy. The data have bad columns around $\sim 4500 \text{ \AA}$.